Fine tuning the hydrophilic–hydrophobic balance in inositols through annulation: An analysis of the hydrogen-bonded architectures of 'annulated inositols'

Goverdhan Mehta* and Saikat Sen

Received 13th September 2005, Accepted 2nd November 2005
First published as an Advance Article on the web 15th November 2005
DOI: 10.1039/b512911g

The crystal structures of conformationally locked, bicyclic cycloalkane-annulated variants of *myo*- and *chiro*-inositols have been analysed, in order to understand their mode of expression of the axial rich conformations and amphiphilicity in the solid state. Thus, while cyclohexa-annulated *myo*- and *chiro*-inositols exhibit a *head-to-head bilayer* molecular assembly, consisting of dimeric or octameric columnar architectures, cyclopenta-annulated *chiro*-inositol shows no such aggregation of the hydrophilic and hydrophobic faces, rather preferring to pack in a manner akin to a hydrophilic inositol. The differences in the two packing modes can be attributed to the size of the hydrocarbon ring, fine-tuning the hydrophilic–hydrophobic balance in the annulated inositols. An analysis of the non-polar molecular surface area (a measure of the intermolecular hydrophobic van der Waals interactions) for all the annulated inositols under study further vindicates the conclusion.

Introduction

Cyclohexane-1,2,3,4,5,6-hexol, in all its nine stereoisomeric forms, constitutes a group of biologically important entities, commonly known as inositols.[1] The diverse biological functions of inositols and their derivatives include intercellular communication, phosphate storage and transfer, anti-cancer activity and involvement in covalent anchoring of proteins to membranes.[1a–c,2] However it is the ability of inositol derivatives, like D-*myo*-inositol-1,4,5-triphosphate [Ins(1,4,5)P_3] and D-*myo*-inositol-1,3,4,5- tetrakisphosphate [Ins(1,3,4,5)P_4], to act as second messengers in signal transduction events (the phosphatidylinositide cascade pathway), through binding to specific receptors and mobilizing Ca^{2+} ions from intracellular stores, that has generated contemporary interest in their chemistry and biology.[1,2] In particular, the quest for unraveling the complex biological mechanisms of the physiological processes, triggered by inositol polyphosphates, has stimulated a search for novel designer analogues for potential use as new pharmaceuticals.[3]

It was in this context that we reported recently the synthesis of 'annulated inositols' as novel entities with several unique attributes.[4] These bicyclic analogues retain the natural configuration of inositols, but are destined to be 'locked' in unnatural *axial-rich* conformations owing to the *trans* fusion of the cyclitol moiety with a hydrocarbon ring ('annulus'). For example, while *myo*-inositol exists in the stable conformation **5** with five equatorial and one axial hydroxyl groups,[5a] the 1,6-annulated *myo*-inositol **1** would be locked in a five axial and one equatorial conformation. In addition, it was expected that the size of the hydrophobic appendage, in the form of an alicyclic ring, could serve as a handle to fine tune the hydrophilic–hydrophobic balance in the otherwise polar inositols. This could in principle serve as a means of modulating the cell membrane permeability and receptor recognition parameters of the inositol moiety. The amphiphilic nature of annulated inositols can also express itself in several intersting and useful physical phenomena like solvent or ion induced gelation, micelle formation for potential use in non-ionic surfactants,[6,7] and liquid crystalline behaviour (like alkyl glycosides).[7,8]

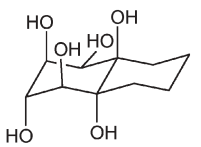

1, cyclohexa-annulated *myo*-inositol (5a/1e)

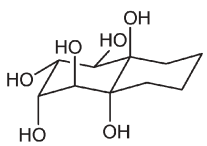

2, cyclohexa-annulated *chiro*-inositol (4a/2e)

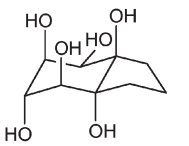

3, cyclopenta-annulated *myo*-inositol (5a/1e)

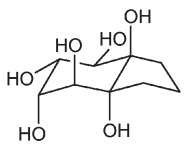

4, cyclopenta-annulated *chiro*-inositol (4a/2e)

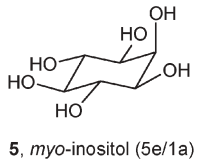

5, *myo*-inositol (5e/1a)

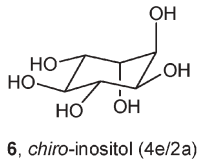

6, *chiro*-inositol (4e/2a)

Availability of these novel inositol variants motivated us to explore the mode of expression of their amphiphilicity and conformational locking of the hydroxyl groups in the solid

Department of Organic Chemistry, Indian Institute of Science, Bangalore 560012, India. E-mail: gm@orgchem.iisc.ernet.in; Fax: +91-80-23600936; Tel: +91 80 2293 2850

state supramolecular architecture. Towards this end, cyclohexa- and cyclopenta-annulated *myo*- (**1** and **3**) and *chiro*-inositols (**2** and **4**) were selected for this study, because they were the analogues of the only two naturally occurring and biologically important inositols (**5** and **6**). It was recognized that the availability of the crystal structures of **5** and **6** in the literature would facilitate appropriate comparisons.[5]

Experimental

Following the synthetic sequence, previously reported, the annulated inositols *rac*-**1**–**4** were obtained as colorless solids, starting with readily available aromatic precursors like tetralin and indane.[4] However, owing to their inherent hygroscopic nature and limited solubility in most organic solvents, obtaining good quality single crystals, suitable for X-ray diffraction analysis, presented a formidable challenge. Eventually crystallization from a solution of 1 : 2 *dry* methanol–ethyl acetate afforded microcrystals of **1**, **2** and **4** suitable for subsequent studies. Despite our best efforts, cyclopenta-annulated *myo*-inositol **3** however gave either a gummy mass or an ill-defined solid, even after several crystallization attempts.

Crystallography

Single crystal X-ray diffraction data were collected on a Bruker AXS SMART APEX CCD diffractometer at 292 K. The X-ray generator was operated at 50 kV and 35 mA using MoK_α radiation. The data was collected with a ω scan width of 0.3°. A total of 606 frames per set were collected using SMART[9] in four different settings of φ (0°, 90°, 180° and 270°) keeping the sample to detector distance at 6.062 cm and the 2θ value fixed at −25°. The data were reduced by SAINTPLUS;[9] an empirical absorption correction was applied using the package SADABS[10] and XPREP[9] was used to determine the space group. The crystal structures were solved by direct methods using SIR92[11] and refined by full-matrix least-squares methods using SHELXL97.[12] Molecular and packing diagrams were generated using ORTEP32,[13] CAMERON[14] and MERCURY[15] respectively. The geometric calculations were done by PARST[16] and PLATON.[17] All the hydrogen atoms were placed in geometrically idealized positions and allowed to ride on their parent atoms with C–H distances in the range 0.97–0.98 Å and $U_{iso}(H) = 1.2U_{eq}(C)$, and O–H distances fixed at 0.82 Å and $U_{iso}(H) = 1.5U_{eq}(O)$. Details of data collection and refinement are given in Table 1.

CCDC reference numbers 282445, 283661 and 283662. For crystallographic data in CIF or other electronic format see DOI: 10.1039/b512911g

Results and discussion

(a) Crystal structure of *rac*-cyclohexa-annulated *myo*-inositol 1

The crystal structure of the C_1-symmetric inositol **1** was solved and refined in the centrosymmetric triclinic space group $P\bar{1}$ ($Z = 2$). Embedded in a rigid *trans*-decalin scaffold, the *myo*-inositol moiety in **1** is locked in a high energy conformation, with five axial and one equatorial (5a/1e) OH groups (Fig. 1).[4]

Table 1 Summary of crystal data, data collection, structure solution and refinement details

	1	2	4
Formula	$C_{10}H_{18}O_6$	$C_{10}H_{18}O_6$	$C_9H_{16}O_6$
M_r	234.24	234.34	220.22
Crystal system	Triclinic	Triclinic	Monoclinic
Space group	$P\bar{1}$	$P\bar{1}$	$P2_1/n$
a/Å	6.113(1)	12.559(4)	7.746(4)
b/Å	7.614(1)	12.916(4)	10.408(5)
c/Å	11.668(2)	13.860(4)	12.556(7)
α/°	102.319(3)	87.959(6)	90
β/°	97.916(3)	87.627(6)	100.061(8)
γ/°	91.829(2)	70.606(6)	90
V/Å^3	524.5(2)	2118.2(11)	996.7(9)
Z	2	8	4
$F(000)$	252	1008	472
ρ_{calc}/g cm^{-3}	1.483	1.469	1.468
μ/mm^{-1}	0.122	0.121	0.124
R_1 [$I > 2\sigma(I)$]	0.0577	0.0499	0.0359
wR_2	0.1353	0.1116	0.0978
GOF	1.017	0.967	1.030
$\Delta\rho_{max/min}$/e Å^{-3}	0.258/−0.244	0.268/−0.202	0.253/−0.228

[a] The CCDC numbers, obtained earlier for **1** and **2** in the context of the report of their synthesis, were 196760 and 196759 respectively.[4]

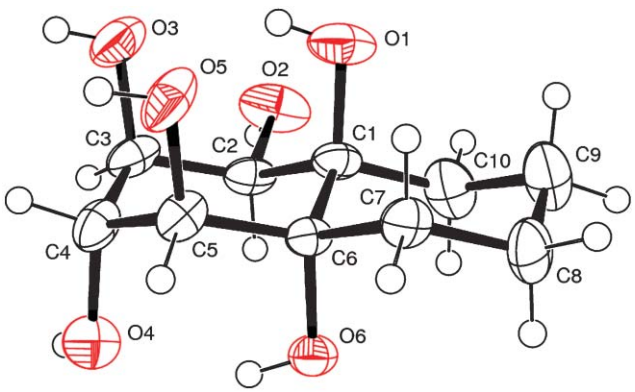

Fig. 1 The ORTEP diagram of **1**, with the atom numering scheme for the asymmetric unit. Displacement ellipsoids for non-H atoms have been drawn at the 50% probability level.

Owing to the resulting non-bonding 1,3-diaxial interactions between the hydroxyl groups, particularly at C2, C4 and C6, the cyclohexane ring, containing the inositol moiety, distorts slightly from an ideal chair conformation. This distortion in the inositol framework is evident not only from an analysis of the puckering parameters (q_2 = 0.0307(1) Å, q_3 = −0.5313(1) Å, φ_2 = 139.25(18)°, Q_T= 0.5322(1) Å, θ_2= 176.69(1)°),[18] but also through a comparison of the C–C–C bond angles with those of natural *myo*-inositol (Table 2).[5a]

The unnatural axial rich conformation of the OH groups in **1** also favorably positions the hydroxyl groups (1,3-*syn* diaxial)

Table 2 Comparision of C–C–C bond angles (°) in cyclohexa-annulated (**1**) and natural *myo*-inositol (**5**)

	1	5		1	5
C2–C1–C6	110.3(3)	111.9(3)	C3–C4–C5	113.3(3)	109.3(3)
C2–C3–C4	112.5(3)	111.3(3)	C5–C6–C1	112.7(3)	110.9(3)
C3–C2–C1	113.5(3)	109.4(3)	C6–C5–C4	111.9(3)	113.4(3)

Table 3 Hydrogen bond geometry in cyclohexa-annulated *myo*-inositol **1** (Å, °)

D–H···A	D–H	H···A	D···A	D–H···A
O1–H1O···O3^{i}	0.82	2.22	2.810(4)	129
O1–H1O···O5^{i}	0.82	2.27	2.826(4)	126
O2–H2O···O2^{ii}	0.82	2.18	2.808(4)	134
O3–H3O···O5^{iii}	0.82	1.98	2.782(4)	165
O4–H4O···O5^{iii}	0.82	1.98	2.782(3)	167
O5–H5O···O3^{iv}	0.82	2.02	2.782(4)	154
O6–H6O···O4^{i}	0.82	1.93	2.371(4)	151

Symmetry codes: (i) x, y, z; (ii) $-x+1$, $-y+2$, $-z+1$; (iii) $-x$, $-y+1$, $-z+1$; (iv) $x+1$, y, z.

to participate in intramolecular H-bonding.[19] Thus while O3 and O5 are linked to O1 by a bifurcated intramolecular H-bond on one face, a two-center H-bond connects O4 to O6 on the opposite face (Table 3). A pair of two intermolecular O–H···O hydrogen bonds involving O3 and O5 and each having an $R^2_2(4)$ pattern,[20,21] join two enantiomerically related molecules of **1** to form a centrosymmetric dimer around the inversion center at (0,½,½) (Fig. 2a). The translationally related molecular dimers, in turn, link to each other along the *a*-axis through intermolecular O–H···O hydrogen bonds involving O5 and O4. The resulting self-assembly has thus a columnar architecture, with a polar interior, defined by the hydroxyl groups, and a non-polar exterior, formed by the cyclohexane rings, disposed parallel to each other (Fig. 2b). These columnar architectures are interconnected along the *b*-axis through intermolecular O–H···O bonds, involving the equatorial hydroxyl groups, in a $R^2_2(4)$ pattern.[20,21] The overall supramolecular assembly of **1** shows a distinct separation of the hydrophilic and hydrophobic faces in a bilayer arrangement (Fig. 3).

(b) Crystal structure of *rac*-cyclohexa-annulated *chiro*-inositol 2

The C_1-symmetric cyclohexa-annulated *chiro*-inositol **2** crystallized in the centrosymmetric triclinic space group $P\bar{1}$ (Z = 8). The four crystallographically independent inositol molecules (designated arbitarilily A, B, C and D for the sake of simplifying the description of the crystal packing) in the asymmetric unit occupy general positions in the crystal lattice. Like **1**, the *chiro*-inositol moiety in **2** is locked in a high energy, unnatural conformation with four axial and two equatorial (4a/2e) hydroxyl groups (Fig. 4).[4] Consequently, on account of the non-bonding interactions between the 1,3-diaxially disposed substituents, the cyclohexane ring, containing the inositol framework in **2**, distorts slightly from an ideal chair conformation. This becomes evident from an analysis of the ring puckering parameters,[18] the C–C–C bond angles and the C–C–C–C torsion angles of the inositol moiety in **2** (Table 4). The 4a/2e conformation of **2** also disposes conducively all the axial hydroxyl groups, involving O1···O3, O2···O6 in molecule A, O11···O13, O12···O16 in molecule B, O21···O23, O22···O26 in molecule C, and O31···O33, O32···O36 in molecule D, to participate in intramolecular O–H···O hydrogen bonding (Table 5).[19] The four crystallographically independent molecules (A, B, C and D) are linked through intermolecular O–H···O hydrogen bonds to form a tetrameric unit (Fig. 5a). Two such units are connected through

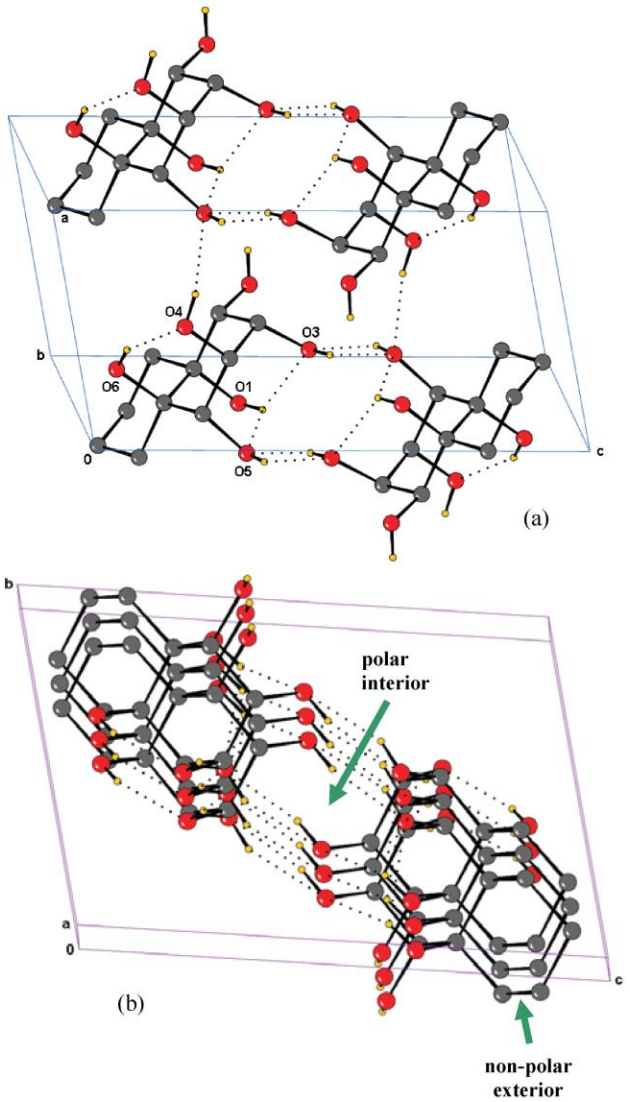

Fig. 2 The columnar packing of the O–H···O hydrogen bonded centrosymmetric dimers (a) of **1**, generating the columnar supramolecular architectures (b), characterized by a non-polar exterior and a polar interior. Click here to access a 3D image of Fig. 2a.

intermolecular O–H···O bonds, involving O4, O10, O14 and O20, across the inversion center at (½,½,0), to generate a centrosymmetric octamer (Fig. 5b). O–H···O H-bonds, involving O11, O12, O17 and O18, join these octameric units to each other along the *a* axis to form, similar to **1**, a columnar molecular self-assembly, having a non-polar exterior and a polar interior. The columnar architectures are, in turn, connected along the *b*-axis through intermolecular O–H···O hydrogen bonds, involving O1, O13, O17 and O19 (Fig. 6). Like **1**, the entire supramolecular assembly of **2** exhibits a definite segregation of the hydrophobic and hydrophilic faces in the form of a bilayer arrangement.

(c) Crystal structure of *rac*-cyclopenta-annulated *chiro*-inositol 4

The C_1-symmetric inositol **4**, a lower homologue of **2**, was found to crystallize in the centrosymmetric monoclinic space group $P2_1/n$ (Z = 4). Like **2**, the *chiro*-inositol moiety in **4**

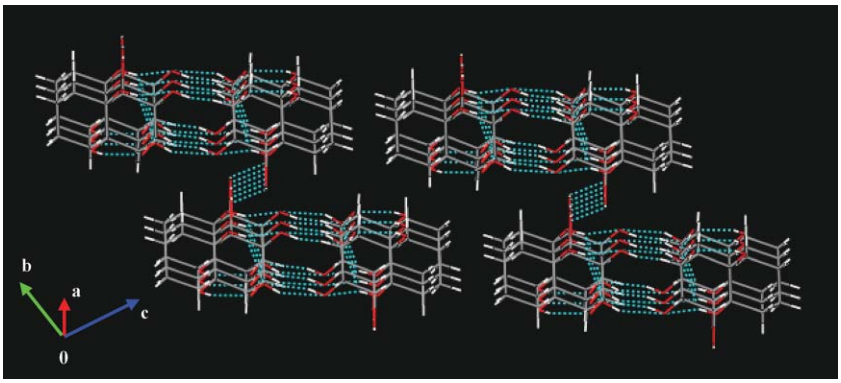

Fig. 3 Crystal packing of **1**, showing the bilayer arrangement of the hydrophilic and hydrophobic faces.

exhibits a 4a/2e conformation of the hydroxyl groups (Fig. 7), with a consequent distortion of the cyclohexane ring from an ideal chair conformation, which is reflected in its puckering parameters (q_2 = 0.055(1) Å, q_3 = −0.564(1) Å, φ_2 = 145(1)°, Q_T = 0.567(1) Å, θ_2 = 174(1)°),[18] C–C–C bond angles and the C–C–C–C torsion angles (Table 6). As might be expected, the intramolecular O–H···O H-bonding pattern in **4** also remains unchanged from that observed in **2** (Table 7). Interestingly, however, the supramolecular organization in **4**, as dictated by the intermolecular O–H···O hydrogen bonds, was in complete constrast to that observed in **1** and **2**. As opposed to the channel-like architecture and the bilayer molecular arrangement seen in the crystal packing of **1** and **2**, cyclopenta-annulated *chiro*-inositol **4** showed no manisfestation of its amphiphilic nature in the supramolecular assembly. All the OH groups in **4** participate in intermolecular O–H···O H-bonding to generate a three-dimensional molecular arrangement, more comparable to one routinely observed for cyclitols and carbohydrates (Fig. 8). Thus, following a $R^2_2(10)$ hydrogen bonding pattern,[20,22] a pair of intermolecular O–H···O H-bonds, involving the equatorial O5 and O4, forms centrosymmetric molecular dimers about (0,½,0) and (½,0,½). These dimers are interconnected by two two-center (O5–H5O···O1 and O3–H3O···O6) and one three-center (involving O2 and O5, O6) hydrogen bonds to effect the final supramolecular assembly in **4**.

Analyzing the differences in the crystal packing of 1, 2 and 4

As expected from a typical polyhydroxylated molecule, the annulated inositols **1**, **2** and **4** self-assemble in the crystalline

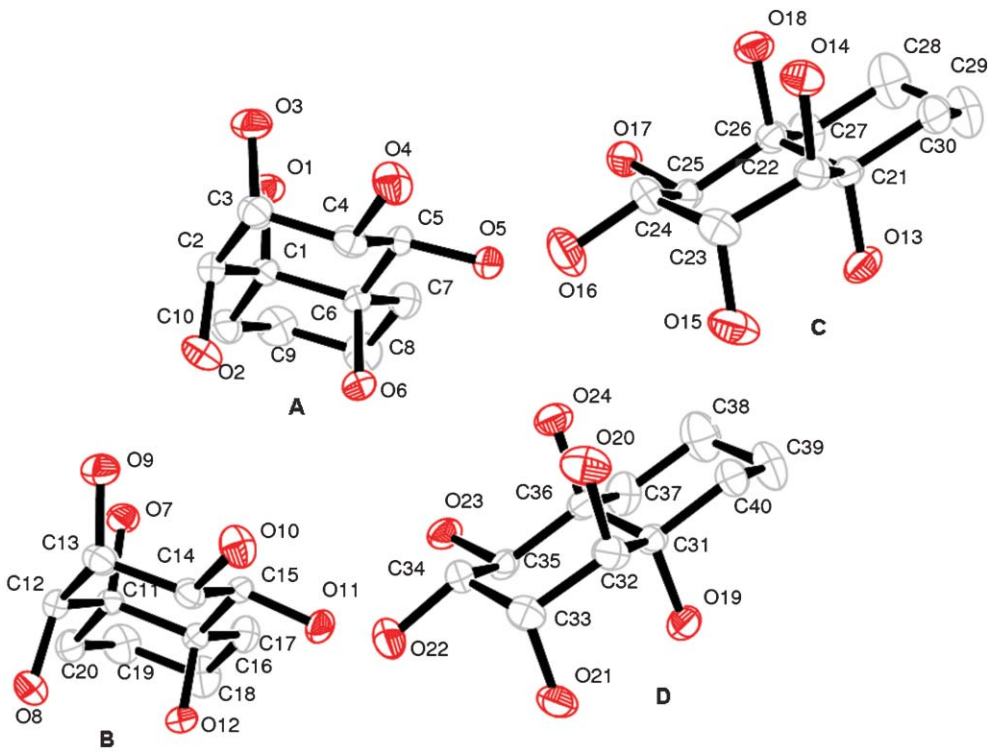

Fig. 4 The ORTEP diagram of **2**, with the atom numering scheme for the asymmetric unit. Displacement ellipsoids have been drawn at the 50% probability level. The hydrogen atoms have been omitted for clarity.

Table 4 The puckering parameters, C–C–C bond angles and C–C–C–C torsion angles of the *chiro*-inositol moiety in **2**

(a) Puckering parameters:[e]

	Mol. A[a]	Mol. B[b]	Mol. C[c]	Mol. D[d]
q_2/Å	0.036(2)	0.034(2)	0.051(2)	0.018(3)
q_3/Å	0.575(2)	−0.566(2)	−0.558(2)	−0.565(2)
φ_2/°	64(3)	108(4)	114(3)	86(7)
Q_T/Å	0.576(2)	0.567(2)	0.560(2)	0.565(2)
θ_2/°	176.4(2)	176.6(2)	174.7(3)	178.2 (3)

(b) C–C–C bond angles (°):[f]

C2–C1–C6	111.6(2) [112.6(1)]	C14–C13–C12	111.1(2)
C3–C2–C1	112.1(2) [110.6(1)]	C14–C15–C16	111.1(2)
C4–C3–C2	110.6(2) [113.1(1)]	C15–C14–C13	112.7(2)
C4–C5–C6	110.7(2) [109.7(1)]	C15–C16–C11	110.0(2)
C5–C4–C3	111.9(2) [110.0(1)]	C22–C21–C26	110.9(2)
C5–C6–C1	109.5(2) [111.3(1)]	C23–C22–C21	112.1(2)
C11–C12–C13	111.8(2)	C23–C24–C25	112.5(2)
C12–C11–C16	111.2(2)	C24–C23–C22	112.6(2)
C24–C25–C26	111.1(2)	C34–C33–C32	111.5(2)
C25–C26–C21	110.0(2)	C34–C35–C36	111.4(2)
C31–C32–C33	111.9(2)	C35–C34–C33	112.0(2)
C32–C31–C36	111.3(2)	C35–C36–C31	110.1(2)

(c) C–C–C–C torsion angles (°):[g]

C2–C1–C6–C5	−55.0(2) [56.2(2)]	C21–C22–C23–C24	−50.9(3)
C2–C3–C4–C5	56.3(2) [−54.8(2)]	C22–C23–C24–C25	51.5(3)
C4–C3–C2–C1	−53.0(3) [51.6(2)]	C23–C22–C21–C26	53.7(2)
C4–C5–C6–C1	57.8(2) [−57.7(2)]	C24–C25–C26–C21	57.7(2)
C6–C1–C2–C3	53.4(2) [−52.1(2)]	C25–C26–C21–C22	−56.8(2)
C6–C5–C4–C3	−59.4(2) [56.7(2)]	C26–C25–C24–C23	−55.4(3)
C11–C12–C13–C14	−52.0(3)	C32–C33–C34–C35	55.1(3)
C12–C11–C16–C15	−56.4(2)	C34–C33–C32–C31	−53.9(3)
C12–C13–C14–C15	53.6(2)	C34–C35–C36–C31	55.9(2)
C13–C12–C11–C16	54.2(2)	C35–C36–C31–C32	−54.6(2)
C14–C15–C16–C11	57.4(2)	C36–C31–C32–C33	54.2(2)
C16–C15–C14–C13	−56.8(2)	C36–C35–C34–C33	−56.7(2)

[a] C-atoms defining the ring: C1, C2, C3, C4, C5, C6. [b] C-atoms defining the ring: C11, C12, C13, C14, C15, C16. [c] C-atoms defining the ring: C21, C22, C23, C24, C25, C26. [d] C-atoms defining the ring: C31, C32, C33, C34, C35, C36. [e] The puckering parameters for natural L-*chiro*-inositol: Q_T = 0.561 Å, θ_2 = 4.4°.[5b] For an ideal cyclohexane conformation, θ_2 = 0 or 180°, so that q_2 = 0 and q_3 = $\pm Q_T$ = 0.63 Å.[18] [f] The values in square brackets indicate the corresponding bond angles in L-*chiro*-inositol.[5b] [g] The values in square brackets indicate the corresponding bond angles in L-*chiro*-inositol.[5b]

lattice, striving to maximize the O–H···O hydrogen bonds possible in the molecule.[23] However it is the maximization of the weaker isotropic van der Waals interactions between the cycloalkane moieties that differentiates the crystal packing in the cyclohexa-annulated inositols **1** and **2** from that observed in the cyclopenta-annulated **4**. The juxtaposition of the hydrophobic faces, together with parallel stacking of the cyclohexane rings, in the crystal structures of **1** and **2** is a clear reflection of the self-assembling process attempting to increase the area of contact (and thus, the extent of van der Waals interactions) between the hydrophobic surfaces as much as possible. Evidently such an attempt leads to a localization of the cooperative O–H···O H-bonding network, extending over all the molecules in the crystal lattice (as seen in **4**, **5** and **6**), to one, involving only the hydrophilic faces in the columnar architectures of **1** and **2**. It is reasonable to believe that the choice between the two types of O–H···O H-bonding patterns

Table 5 Hydrogen bond geometry in cyclohexa-annulated *chiro*-inositol **2** (Å, °)

D–H···A	D–H	H···A	D···A	D–H···A
O1–H1O···O3^{i}	0.82	1.92	2.654(3)	148
O2–H2O···O9^{i}	0.82	2.10	2.911(3)	170
O3–H3O···O8^{ii}	0.82	2.24	3.010(3)	157
O4–H4O···O16^{i}	0.82	2.18	2.930(3)	151
O5–H5O···O24^{i}	0.82	1.93	2.686(2)	153
O6–H6O···O2^{i}	0.82	2.00	2.733(2)	149
O7–H7O···O19^{iii}	0.82	2.01	2.829(2)	174
O8–H8O···O12^{i}	0.82	1.98	2.657(2)	140
O9–H9O···O7^{i}	0.82	2.01	2.710(3)	143
O10–H10O···O14^{iv}	0.82	1.97	2.789(3)	175
O11–H11O···O23^{i}	0.82	1.91	2.706(3)	165
O12–H12O···O17^{v}	0.82	1.93	2.695(2)	155
O13–H13O···O1^{vi}	0.82	2.01	2.827(3)	173
O14–H14O···O18^{i}	0.91(3)	1.83(3)	2.634(3)	147(3)
O15–H15O···O13^{i}	0.82	2.07	2.751(3)	140
O16–H16O···O20^{i}	0.82	2.32	3.121(2)	164
O17–H17O···O5^{i}	0.82	1.92	2.735(3)	171
O18–H18O···O11^{i}	0.82	1.91	2.638(2)	148
O19–H19O···O21^{i}	0.82	1.94	2.652(3)	144
O20–H20O···O4^{iv}	0.82	1.91	2.720(3)	172
O21–H21O···O14^{v}	0.82	2.02	2.828(3)	169
O22–H22O···O10^{i}	0.82	2.13	2.943(3)	169
O23–H23O···O6^{i}	0.82	1.94	2.717(2)	157
O24–H24O···O20^{i}	0.82	1.92	2.660(3)	149

Symmetry codes: (i) x, y, z; (ii) $x-1$, y, z; (iii) x, $y+1$, z; (iv) $-x+1$, $-y+1$, $-z$; (v) $x+1$, y, z; (vi) x, $y-1$, z.

is dictated primarily by the contribution that the weak van der Waals interactions may have relative to the much stronger O–H···O hydrogen bonds, in the crystal packing of an annulated inositol. This, evidently, will depend on the effective hydrophobic surface presented by the annulated inositol on account of the cycloalkane appendage. To probe this point further, we decided to compare the relative contributions of the non-polar surface to the total molecular surface area in the inositols **1**, **2** and **4**.

All molecular surface calculations for **1**, **2** and **4** were performed with VEGA ZZ 2.0.4.1,[24] using the atomic coordinates, as determined by single crystal X-ray crystallography, as the input. The polar surface area (PSA) for the different annulated inositols was calculated considering the polar (O and H bonded to O) and the non-polar (C and H bonded to C) atom surfaces. The molecular surface data, calculated for **4**, was compared further with that obtained using the atomic coordinates from the Gaussian 03[25] optimized (B3LYP/6-31G(p,d)) structure of cyclopenta-annulated *myo*-inositol **3** (Fig. 9). The results of the molecular surface calculations have been enumerated in Table 8.

As might be expected intuitively, the non-polar surface area of the cyclohexa-annulated inositols **1** and **2** contributes to nearly half of the total molecular surface. This therefore represents a situation in which the hydrophobic character of the amphiphilic annulated inositol is almost as dominant as its hydrophilic nature, and is manifested in the molecular self-assembly process in **1** and **2** attempting to maximize not only the strong O–H···O H-bonds, but also the weak van der Waals interactions. Reducing the size of the cycloalkane ring by a methylene unit, as in **3** and **4**, causes the non-polar surface to shrink by about 10%, with a consequent diminution in the hydrophobic character. This shifts the hydrophilic–hydrophobic balance in the annulated inositol in favour of the former,

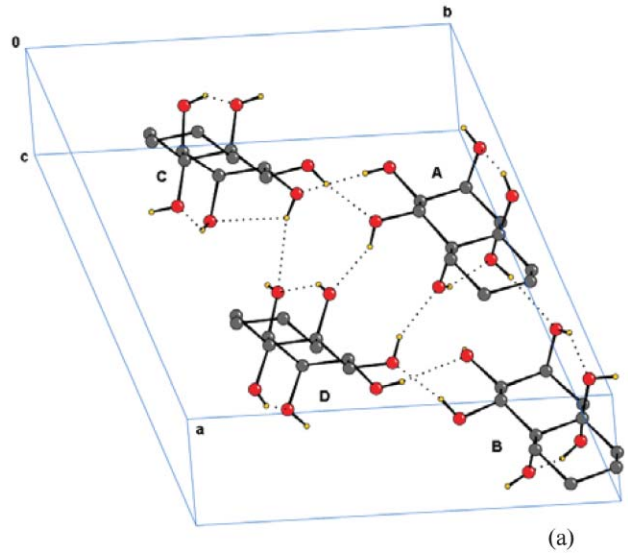

(a)

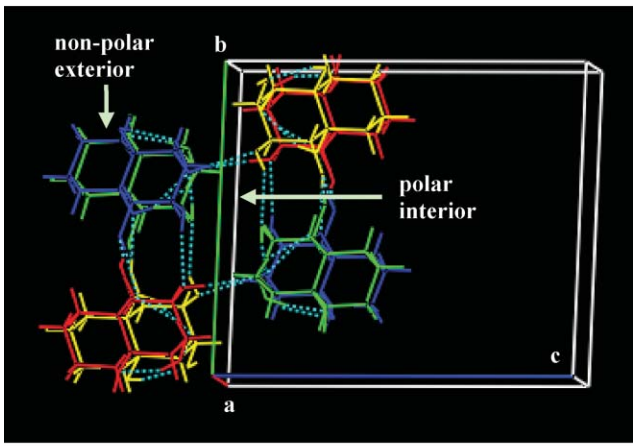

(b)

Fig. 5 (a) Details of the O–H···O hydrogen bonding within the tetrameric unit, formed by the four symmetry independent molecules of **2**. Click here to access a 3D image of Fig. 5a. Two such tetrameric units form a hydrogen bonded centrosymmetric octamer (b), presenting a non-polar exterior and a polar interior. The inositol molecules in (b) have been colored according to their symmetry equivalence (color code: mol. A, yellow; mol. B, red; mol. C, green; mol. D, blue).

and is reflected, for example, in the crystal packing of **4** being more akin to that of any hydrophilic inositol.

Conclusions

The design and synthesis of annulated inositols was conceptualized for the creation of novel entities which would not only be locked in the unnatural, axial-rich conformation of the inositol moiety, but also provide a means of generating amphiphilicity in the otherwise hydrophilic inositols. The present paper studies the manner in which these attributes express themselves in the solid state self-assembly of annulated inositols. The *head-to-head bilayer structures*, observed in the crystal packing of cyclohexa-annulated *chiro*- and *myo*-inositols, is reminiscent of the supramolecular assembly seen in the crystal structures of alkyl glycosides.[7] It would also be

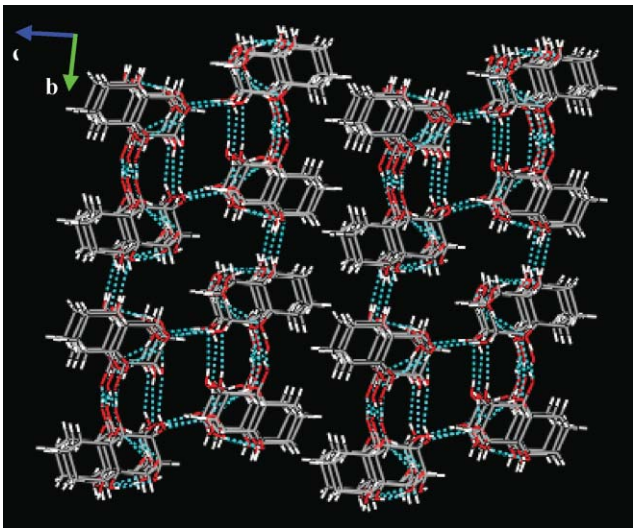

Fig. 6 Crystal packing in cyclohexa-annulated *chiro*-inositol **2**, showing the columnar architectures formed by the supramolecular octamers (detailed in Fig. 5b), and the bilayer arrangement of the hydrophilic and hydrophobic faces.

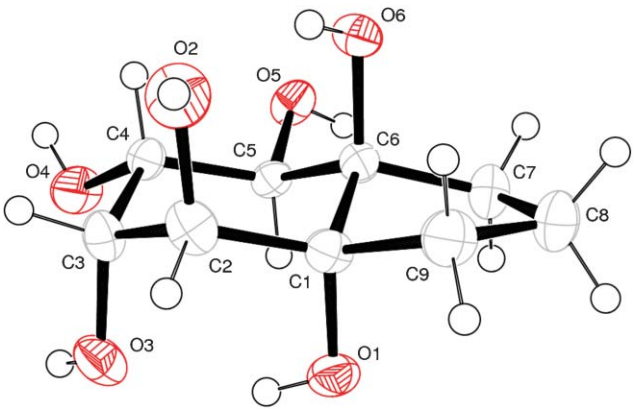

Fig. 7 The ORTEP diagram of **4**, with the atom numering scheme for the assymetric unit. Displacement ellipsoids for non-H atoms have been drawn at the 50% probability level.

Table 6 The C–C–C bond angles (Å) and C–C–C–C torsion angles (°) of the *chiro*-inositol moiety in **4**

C1–C2–C3	110.0(1)	C1–C2–C3–C4	−52.1(1)
C2–C1–C6	111.4(1)	C2–C3–C4–C5	51.6(1)
C4–C3–C2	112.9(1)	C2–C1–C6–C5	−59.4(1)
C5–C4–C3	113.1(1)	C4–C5–C6–C1	56.8(1)
C5–C6–C1	110.3(1)	C6–C1–C2–C3	56.2(1)
C6–C5–C4	110.5(1)	C6–C5–C4–C3	−53.4(1)

worth referring at this point to the crystal packing of *rac*-cyclohexa-annulated methyl-α-gulopyranoside, which like **1** and **2**, shows a columnar architecture with a hydrophilic interior and a hydrophobic exterior.[26] This *head-to-head bilayer* molecular assembly disappears completely in cyclopenta-annulated **4**, which shows a crystal packing, more akin to that of a hydrophilic inositol. The current study provides therefore a direct demonstration of the potential ability of cycloalkane annulation to serve as a tool in fine-tuning the

Table 7 Bond geometry in cyclopenta-annulated *chiro*-inositol **4** (Å, °)

D–H···A	D–H	H···A	D···A	D–H···A
O1–H1O···O3^{i}	0.82	1.88	2.617(2)	150
O2–H2O···O5^{ii}	0.82	2.18	2.854(2)	140
O2–H2O···O6^{ii}	0.82	2.42	3.119(2)	144
O3–H3O···O6^{iii}	0.82	2.08	2.864(2)	159
O4–H4O···O5^{iv}	0.82	2.01	2.737(2)	148
O5–H5O···O1^{v}	0.82	1.89	2.708(2)	174
O6–H6O···O2^{i}	0.82	1.92	2.650(2)	149

Symmetry codes: (i) x, y, z; (ii) $-x - ½$, $y + ½$, $-z + ½ + 1$; (iii) $x + ½$, $-y + ½ + 1$, $z + ½$; (iv) $-x$, $-y + 1$, $-z + 2$; (v) $-x - ½$, $y - ½$, $-z + ½ + 1$.

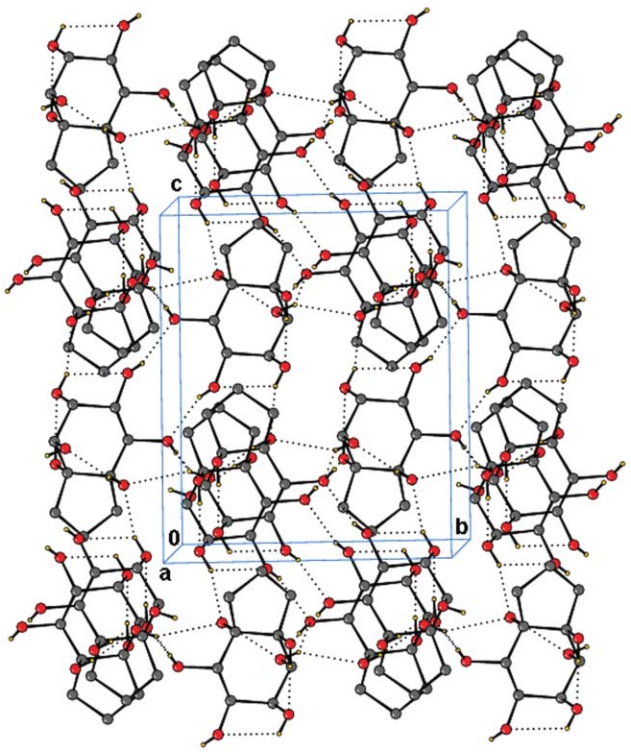

Fig. 8 Crystal packing in cyclopenta-annulated *chiro*-inositol **4**. The hydrogen atoms, connected to C, have been omitted for clarity. Click here to access a 3D image of Fig. 8.

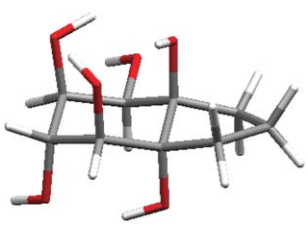

Fig. 9 The Gaussian 03 optimized structure of cyclopenta-annulated *myo*-inositol **3**.

hydrophilic–hydrophobic balance in polar molecules. The results are significant, and can be used as leads towards the design of new molecular materials.

Table 8 Molecular surface area calculations on **1**, **2**, **3** and **4**[a]

Mol.	Total molecular surface area (S_t)/Å^2	Polar surface area, PSA (S_1)/Å^2	Non-polar surface (S_2)/Å^2	S_1/S_2
1	539.4	277.7	261.7	1.1
2[b]	539.1	285.6	253.5	1.1
3	517.7	293.2	224.7	1.3
4	524.0	296.2	227.8	1.3

[a] Probe radius = 1.4 Å. [b] The values are averaged over the four independent molecules in the asymmetric unit.

Acknowledgements

We thank Dr Senaiar S. Ramesh and Mr Mrinal K. Bera for providing access to the crystal data (**1** and **2**) and the crystalline samples (**4**) of their synthetic compounds for further analysis, Ms Manju Sharma for her help in the Gaussian 03 calculations, and DST, India for the CCD facility at IISc, Bangalore. GM thanks CSIR, India for research support and the award of the Bhatnagar Fellowship.

References and notes

1 For selected reviews dealing with the chemistry and biology of inositols, see: (*a*) M. J. Berridge and R. F. Irvine, *Nature (London)*, 1984, **312**, 315–321; (*b*) M. J. Berridge and R. F. Irvine, *Nature (London)*, 1989, **341**, 197–205; (*c*) B. V. L. Potter, *Nat. Prod. Rep.*, 1990, 1–24; (*d*) B. V. L. Potter and D. Lampe, *Angew. Chem., Int. Ed. Engl.*, 1995, **34**, 1933–1972; (*e*) K. Hinterding, D. A. Díaz and H. Waldmann, *Angew. Chem., Int. Ed.*, 1998, **37**, 688–749; (*f*) Y.-T. Chang, G. R. Rosania and S.-K. Chung, *Expert Opin. Ther. Pat.*, 2001, **11**, 45–59; (*g*) S. B. Shears, *Cell. Signalling*, 2001, **13**, 151–158; (*h*) R. Irvine, *Curr. Biol.*, 2001, **11**, R172–174; (*i*) N. R. Leslie and C. P. Downes, *Cell. Signalling*, 2002, **14**, 285–295; (*j*) S. K. Fisher, J. E. Novak and B. W. Agranoff, *J. Neurochem.*, 2002, **82**, 736–754; (*k*) I. Vucenik and A. M. Shamsuddin, *J. Nutr.*, 2003, **133**, 3778S–3784S; (*l*) K. Pattni and G. Banting, *Cell. Signalling*, 2004, **16**, 643–654.
2 M. J. Berridge, *Nature (London)*, 1993, **361**, 315–325.
3 For some selected references on inositol analogues, see: (*a*) A. B. Cheikh, L. E. Craine, J. Zemlicka and M. H. Heeg, *Carbohydr. Res.*, 1990, **199**, 19–30; (*b*) A. P. Kozikowski, A. H. Fauq, G. Powis and D. C. Melder, *J. Am. Chem. Soc.*, 1990, **112**, 4528–4531; (*c*) A. M. Riley and B. V. L. Potter, *J. Org. Chem.*, 1995, **60**, 4970–4971; (*d*) D. J. Jenkins, A. M. Riley and B. V. L. Potter, *J. Org. Chem.*, 1996, **61**, 7719–7726; (*e*) C. Liu and B. V. L. Potter, *J. Org. Chem.*, 1997, **62**, 8335–8340; (*f*) A. M. Riley and B. V. L. Potter, *Tetrahedron Lett.*, 1999, **40**, 2213–2216; (*g*) A. Schnaars and C. Schultz, *Tetrahedron*, 2001, **57**, 519–524; (*h*) H. Sun, G. B. Reddy, C. George, E. J. Meuillet, M. Berggren, G. Powis and A. P. Kozikowski, *Tetrahedron Lett.*, 2002, **43**, 2835–2838.
4 G. Mehta, S. S. Ramesh and M. K. Bera, *Chem. Eur. J.*, 2003, **9**, 2264–2272.
5 (*a*) I. N. Rabinowitz and J. Kraut, *Acta Crystallogr.*, 1964, **17**, 159–168 (the crystal structure of *myo*-inositol); (*b*) G. A. Jeffrey and Y. Yeon, *Carbohydr. Res.*, 1987, **159**, 211–216 (the crystal structure of L-*chiro*-inositol).
6 A. T. Florence and J. A. Rogers, *J. Pharm. Pharmacol.*, 1971, **23**, 233–251.
7 G. A. Jeffrey, *Acta Crystallogr., Sect. B*, 1990, **46**, 89–103.
8 (*a*) G. A. Jeffrey and S. Bhattacharjee, *Carbohydr. Res.*, 1983, **115**, 53–58; (*b*) G. A. Jeffrey, *Mol. Cryst. Liq. Cryst.*, 1984, **110**, 221–237.
9 *SMART (V6.028), SAINT (V6.02), XPREP*, Bruker AXS Inc., Madison, WI, USA, 1998.
10 G. M. Sheldrick, *SADABS*, University of Göttingen, Germany, 1996.
11 A. Altomare, G. Cascarano, C. Giacovazzo and A. Guagliardi, *J. Appl. Crystallogr.*, 1993, **26**, 343.

12 G. M. Sheldrick, *SHELXL97*, University of Göttingen, Germany, 1997.
13 L. J. Farrugia, *J. Appl. Crystallogr.*, 1997, **30**, 565.
14 D. M. Watkin, L. Pearce and C. K. Prout, *CAMERON – A Molecular Graphics Package*, Chemical Crystallography Laboratory, University of Oxford, Oxford, 1993.
15 I. J. Bruno, J. C. Cole, P. R. Edgington, M. K. Kessler, C. F. Macrae, P. McCabe, J. Pearson and R. Taylor, *Acta Crystallogr., Sect. B*, 2002, **58**, 389–397.
16 (*a*) M. Nardelli, *Comput. Chem.*, 1983, **7**, 95–97; (*b*) M. Nardelli, *J. Appl. Crystallogr.*, 1995, **28**, 659.
17 (*a*) A. L. Spek, *Acta Crystallogr., Sect. A*, 1990, **46**, C34; (*b*) A. L. Spek, *PLATON, A Multipurpose Crystallographic Tool*. Utrecht University, Utrecht, The Netherlands, 1998.
18 D. Cremer and J. A. Pople, *J. Am. Chem. Soc.*, 1975, **97**, 1354–1358.
19 (*a*) G. A. Jeffrey and W. Saenger, *Hydrogen Bonding in Biological Structures*, Springer-Verlag, New York, 1991; (*b*) G. A. Jeffrey, *An Introduction to Hydrogen Bonding*; Oxford University Press, Oxford, UK, 1997.
20 (*a*) M. C. Etter, *Acc. Chem. Res.*, 1990, **23**, 120–126; (*b*) M. C. Etter, J. C. MacDonald and J. Berstein, *Acta Crystallogr., Sect. B*, 1990, **46**, 256–262; (*c*) J. Bernstein, R. E. Davis, L. Shimoni and N.-L. Chang, *Angew. Chem., Int. Ed. Engl.*, 1995, **34**, 1555–1573.
21 For some examples on the $R^2_2(4)$ H-bonding motif, see: (*a*) C. Glidewell, C. M. Zakaria and G. Ferguson, *Acta Crystallogr., Sect. C*, 1996, **52**, 1305–1309; (*b*) G. Ferguson and C. Glidewell, *Acta Crystallogr., Sect. C*, 1996, **52**, 3057–3062; (*c*) C. Glidewell, R. B. Klar, P. Lightfoot, C. M. Zakaria and G. Ferguson, *Acta Crystallogr., Sect. B*, 1996, **52**, 110–126.
22 The most common hydrogen-bonding motif in the fully O–H···O H-bonded crystal structures of vicinal diols $C_nH_m(OH)_2$ was found to be an $R^2_2(10)$ dimer, which can be linked in a variety of ways to form one-, two- and three-dimensional packing patterns, see: C. P. Brock, *Acta Crystallogr., Sect. B*, 2002, **58**, 1025–1031.
23 J. M. Robertson, *Organic Crystals and Molecules*, Cornell University Press, Ithaca, New York, 1953.
24 (*a*) A. Pedretti, L. Villa and G. Vistoli, *J. Mol. Graphics*, 2002, **21**, 47–49; (*b*) A. Pedretti, L. Villa and G. Vistoli, *Theor. Chem. Acc.*, 2003, **109**, 229–232; (*c*) A. Pedretti, L. Villa and G. Vistoli, *J. Comput. Aided Mol. Des.*, 2004, **18**, 167–173.
25 M. J. Frisch, G. W. Trucks, H. B. Schlegel, G. E. Scuseria, M. A. Robb, J. R. Cheeseman, J. A. Montgomery, Jr., T. Vreven, K. N. Kudin, J. C. Burant, J. M. Millam, S. S. Iyengar, J. Tomasi, V. Barone, B. Mennucci, M. Cossi, G. Scalmani, N. Rega, G. A. Petersson, H. Nakatsuji, M. Hada, M. Ehara, K. Toyota, R. Fukuda, J. Hasegawa, M. Ishida, T. Nakajima, Y. Honda, O. Kitao, H. Nakai, M. Klene, X. Li, J. E. Knox, H. P. Hratchian, J. B. Cross, C. Adamo, J. Jaramillo, R. Gomperts, R. E. Stratmann, O. Yazyev, A. J. Austin, R. Cammi, C. Pomelli, J. W. Ochterski, P. Y. Ayala, K. Morokuma, G. A. Voth, P. Salvador, J. J. Dannenberg, V. G. Zakrzewski, S. Dapprich, A. D. Daniels, M. C. Strain, O. Farkas, D. K. Malick, A. D. Rabuck, K. Raghavachari, J. B. Foresman, J. V. Ortiz, Q. Cui, A. G. Baboul, S. Clifford, J. Cioslowski, B. B. Stefanov, G. Liu, A. Liashenko, P. Piskorz, I. Komaromi, R. L. Martin, D. J. Fox, T. Keith, M. A. Al-Laham, C. Y. Peng, A. Nanayakkara, M. Challacombe, P. M. W. Gill, B. Johnson, W. Chen, M. W. Wong, C. Gonzalez and J. A. Pople, *Gaussian 03, revision C.02*, Gaussian, Inc., Wallingford, CT, 2004.
26 G. Mehta and S. S. Ramesh, *Eur. J. Org. Chem.*, 2005, 2225–2238.